Energy & Environmental Science

Cite this: *Energy Environ. Sci.*, 2011, **4**, 4929

www.rsc.org/ees

COMMUNICATION

Facile colloidal synthesis of quinary $CuIn_{1-x}Ga_x(S_ySe_{1-y})_2$ (CIGSSe) nanocrystal inks with tunable band gaps for use in low-cost photovoltaics†

Shu-Hao Chang,[a] Ming-Yi Chiang,[a] Chien-Chih Chiang,[b] Fang-Wei Yuan,[a] Chia-Yu Chen,[a] Bo-Cheng Chiu,[a] Tzu-Lun Kao,[a] Chi-Huang Lai[c] and Hsing-Yu Tuan*[a]

Received 11th August 2011, Accepted 26th September 2011
DOI: 10.1039/c1ee02341a

We report, for the first time, colloidal synthesis of quinary $CuIn_{1-x}Ga_x(S_ySe_{1-y})_2$ (CIGSSe) nanocrystals across the entire composition range (x,y) = 0 to 1 with band gaps tunable in the range of 0.98 to 2.40 eV by facile chemical synthesis. As a proof-of-concept, thin-film solar cells made by using the CIGSSe nanocrystal inks as an absorber layer precursor exhibited an efficiency over 1% under AM 1.5 illumination.

Colloidal semiconductor nanocrystals have excellent optoelectronic properties, photo-stability, and long-term dispersion stability, making them well-suited for incorporation into photovoltaic device fabrication processes.[1] The utilization of solution-processable nanocrystals permits the use of relatively low-cost manufacturing equipment so as to greatly reduce the overall fabrication cost of solar cells.[2] One representative example is that absorber layers can be facilely prepared by deposition of a nanocrystal solution, the so-called nanocrystal inks, on a substrate *via* a variety of solution-based techniques, such as spray deposition, dip-coating, slip casting, inject-printing, screen printing *etc.*,[3] thereby enabling the development of high-throughput roll-to-roll processing.

$CuIn_{1-x}Ga_x(S_ySe_{1-y})_2$ (CIGSSe) has a high optical absorption coefficient, good photodurability, and the desired optical band-gap range, representing as a great light-harvesting material for thin film solar cells.[4] The power-conversion-efficiency of 16.03% CIGSSe-based solar cells was recently achieved on a 30 cm × 30 cm sized sub-module, exhibiting an efficiency comparable to crystalline Si-based photovoltaics.[5] Band-gap energies of the CIGSSe system can be tuned from 0.98 to 2.40 eV, wider than its quaternary systems including CISSe (0.98 to 1.46 eV), CIGS (1.46 to 2.4 eV), CIGSe (0.98 to 1.68 eV), and CGSSe (1.68 to 2.4 eV), providing advantageous characteristics for use in double-graded or tandem cell designs.[6] On the other hand, utilizing colloidal CIGSSe nanocrystals for use as an absorber layer precursor could achieve quinary composition uniformity over a large device area that is hardly attainable by vacuum-deposited techniques.[7] However, the synthesis of CIGSSe nanocrystals represents significant difficulty in synthesis due to the complicated phase diagram of quinary alloys. Achieving compositional and structural control of CIGSSe nanocrystals requires precise control of the atomic ratios for both In/Ga and S/Se in the synthesis, which is more challenging than that of quaternary or ternary nanocrystals[8] in which one set of alloying elements (*e.g.*, In and Ga for $CuIn_xGa_{1-x}S_2$[8e]) was stoichiometry-adjusted in most cases. To the best of our knowledge, no CIGSSe nanocrystal synthesis across the entire composition range has been reported.

[a]*Department of Chemical Engineering, National Tsing Hua University, Hsinchu, Taiwan, 30013, Republic of China. E-mail: hytuan@che.nthu.edu.tw; Fax: +886-3-571-5408; Tel: +886-3-571-5408*
[b]*Green Energy & Environment Research Laboratories (GEL), Industrial Technology Research Institute (ITRI), Hsinchu, Taiwan, 31040, Republic of China*
[c]*Department of Materials Science and Engineering, National Tsing Hua University, Hsinchu, Taiwan, 30013, Republic of China*

† Electronic supplementary information (ESI) available: Detailed experimental procedures, supporting figures and tables. See DOI: 10.1039/c1ee02341a

Broader context

Quinary $CuIn_{1-x}Ga_x(S_ySe_{1-y})_2$ (CIGSSe)-based solar cells exhibit module efficiency comparable to crystalline Si-based photovoltaics. Their tunable band-gap energy from 0.98 to 2.40 eV provides advantageous characteristics for use in double-graded or tandem cell designs. CIGSSe nanocrystal is an important material since utilizing them as an absorber precursor can achieve composition uniformity over a large device area that is hardly achievable by vacuum-based techniques, and in addition, permits the use of relatively low-cost and high-throughput manufacturing equipment for device fabrication processing. However, due to the complicated phase diagram of quinary alloys, achieving compositional and structural control for CIGSSe nanocrystals is much more challenging than quaternary and ternary compounds, making its significant synthesis difficult. We report here that CIGSSe nanocrystal synthesis with controllable composition and band gaps can be achieved by a facile chemical method. Thin-film solar cells made by the CIGSSe nanocrystal inks yielded an efficiency over 1%, demonstrating that quinary CIGSSe nanocrystal is a promising new type of absorber layer precursor.

We here report the synthesis of CIGSSe nanocrystals with controllable In/Ga and S/Se ratio and band gaps by facile heating-up synthesis. CIGSSe nanocrystals were used as absorber layer precursors for thin-film solar devices, which yielded cell efficiency over 1% under AM 1.5 illumination.

Nanocrystals were synthesized by thermal decomposition of CuCl, $InCl_3$, $GaCl_3$, S, and Se in the presence of oleylamine at 265 °C. Oleylamine serves as a solvent, coordinating agent, capping reagent, and may reduce the precursors' activity difference. By varying the In/Ga and S/Se reactant ratio in the reaction, the composition of CIGSSe could be adjusted and its optical band-gap could be correspondingly engineered. This strategy provides a facile route to precisely control the ratios of both In/Ga and S/Se in the CIGSSe nanocrystals in one-pot reactions. The band gap energies of nanocrystals are tunable from 0.98 to 2.40 eV, giving almost the widest range that the series of CIGSSe nanocrystals can achieve. In addition, the high-yield heating-up synthesis gives away from the need of complicated chemicals and experimental instruments for processing, thereby providing superior advantages for commercial production.

Fig. 1 shows the synthesis result of $CuIn_{0.5}Ga_{0.5}(S_{0.5}Se_{0.5})_2$ nanocrystals from the developed approach. XRD patterns show nanocrystals with a chalcopyrite-phase. No other impurities, such as binary sulfides or selenides related to reactants were detected, indicating the phase purity of the product. The size and morphology of as-synthesized nanocrystals were examined by transmission electron microscopy (TEM) (Fig. 1b). The $CuIn_{0.5}Ga_{0.5}(S_{0.5}Se_{0.5})_2$ nanocrystals have an average diameter of 16 ± 5 nm and a slightly irregular faceted shape. The selected-area electron diffraction pattern (SAED) of a field of nanocrystals shows three main diffraction rings, in agreement with the (112), (220), and (312) of the chalcopyrite phase, respectively. High resolution TEM (HRTEM) (Fig. 1c) shows the high-degree crystallinity of the nanocrystals. The atomic ratio of Cu : In : Ga : S : Se determined by energy-dispersive X-ray spectroscopy (EDS) of nanocrystals is nearly 0.25 : 0.125 : 0.125 : 0.25 : 0.25. STEM-EDS mapping of particles (Fig. S1† is available in the ESI) confirms that the five elements are equally distributed, indicating nanocrystals uniformly alloyed. Electronic states of each element were determined by XPS, giving the respective chemical valence: Cu: +1; In: +3; Ga: +3; S: −2; Se: −2. (Fig. S2†). The developed heating-up approach is easily scalable to gram-quantity of nanocrystal production. Fig. 1f shows 1.34 g of dried $CuIn_{0.5}Ga_{0.5}(S_{0.5}Se_{0.5})_2$ nanocrystal powder obtained from one-pot reaction. The quality of nanocrystals remains the same as those from milligram-scale reactions as confirmed by detail characterization (Fig. S3†).

The In/Ga and S/Se ratio of CIGSSe nanocrystals could be controlled by varying the In/Ga and S/Se reactant ratio in the synthesis. Fig. 2a shows the XRD patterns of nanocrystals with different compositions together with the indexing of major peaks. As the Ga and S content increases, the diffraction peaks gradually

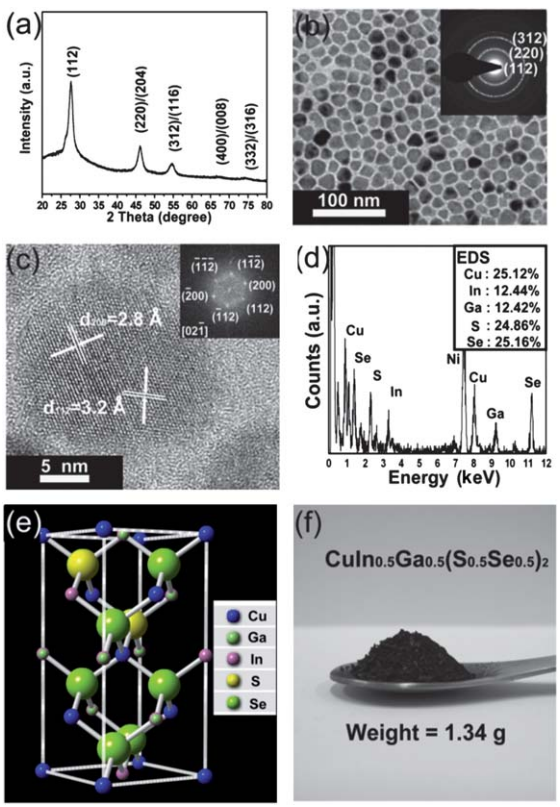

Fig. 1 (a) XRD pattern, (b) TEM image (inset: indexed SAED pattern), (c) HRTEM image (inset: the corresponding FFT pattern), (d) EDS, (e) simulated unit cell, and (f) powder photograph of $CuIn_{0.5}Ga_{0.5}(S_{0.5}Se_{0.5})_2$ nanocrystals.

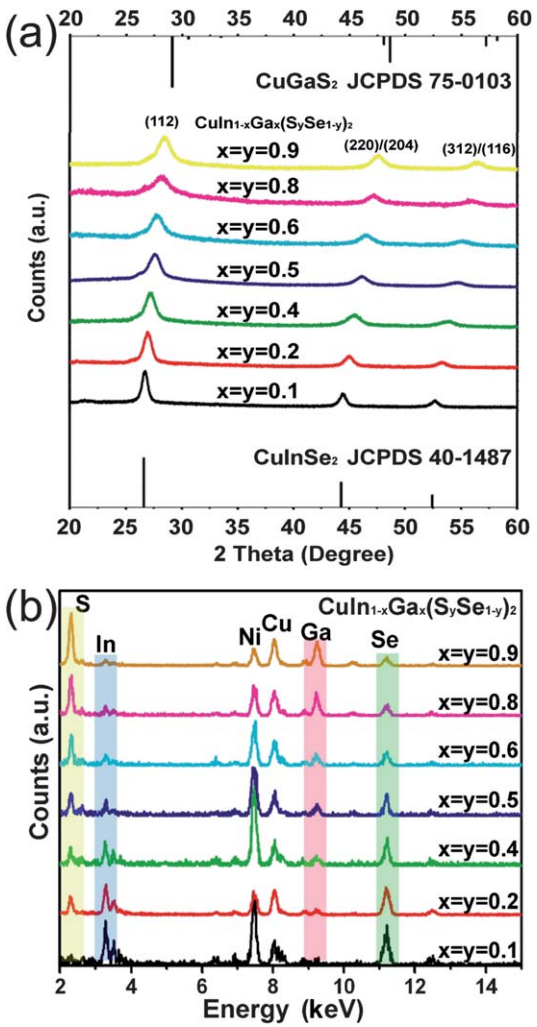

Fig. 2 (a) XRD patterns and (b) EDS of a series of CIGSSe nanocrystal samples with varying compositions.

shift toward larger angles. A gradual decrease in lattice spacing along the *a*-axis (from 5.782 Å ($CuInSe_2$) to 5.349 Å ($CuGaS_2$)) and *c*-axis (from 11.619 Å ($CuInSe_2$) to 10.470 Å ($CuGaS_2$)) was observed with the decrease of In and Se content in the nanocrystals. The relationship between the nanocrystal lattice parameter and composition is consistent with Vegard's law (Fig. S4 and Table S1†),[9] showing the formation of alloyed nanocrystals with homogeneous distribution of CIGSSe matrix. EDS of a field of CIGSSe nanocrystals with varying compositions shows that as the Ga and S content was increased in the reactants, the intensities of the S and Ga peaks were increased. The details of quantitative elemental EDS analysis of these nanocrystals are listed in Table S4†. TEM images of CIGSSe nanocrystals are shown in Fig. S5 and S6†. The average particle sizes of nanocrystals were in the range of 15 to 20 nm for all compositions.

We have characterized the band gap energy information of CIGSSe nanocrystals in both experimental and theoretical ways since the information is very important for their future implementation in electronic devices. Fig. 3a shows optical absorbance spectra of CIGSSe nanocrystals dispersed in toluene. The shift of the spectra is clearly originated from composition-varied CIGSSe nanocrystals, rather than other systems such as a core–shell structure. The systematic blue-shift of the absorption onset as the Ga and S content increases is due to the wider band gap of $CuGaS_2$ relative to that of $CuInSe_2$. Fig. 3b shows a photograph of different CIGSSe nanocrystal solutions at the same molar concentration. The optical band-gap energies were determined by the intercepts of the tangent of the absorption spectra (see Fig. S7† for the details of band gap determination), and the values are listed in Fig. 3a. In addition, cyclic voltammetry (CV) was used to determine the band edge position of nanocrystals. The HOMO and LUMO energy levels can be derived from the onset oxidation potential (E_{ox}) and onset reduction potential (E_{red}), respectively. Fig. 3c shows the CV curves of a series of CIGSSe nanocrystals. As x and y increase for CIGSSe nanocrystals, the onset reduction potentials were shifted to the lower voltage and the onset oxidation potentials were shifted to the higher voltage. The complete set of band-gap positions and values of nanocrystals is shown in Fig. 3d (see Fig. S8† for the details of HOMO and LUMO position determination).

Theoretically, the band-gap energies of quinary $CuIn_{1-x}Ga_x(S_ySe_{1-y})_2$ depending on $0 \leqq x \leqq 1$ and on $0 \leqq y \leqq 1$ could be determined based on binary models, yielding an expression:[10]

$$E_g^{CIGSSe}(x,y) = (1-y)[(1-x)E_g^{CISSe}(y) + xE_g^{CGSSe}(y) - b^{CIGSe}x(1-x)] + y[(1-x)E_g^{CISSe}(y) + xE_g^{CGSSe}(y) - b^{CIGS}x(1-x)] \quad (1)$$

Applying the band gap equations and the optical bowing constants of CISSe, CGSSe, CIGSe, and CIGS (Table S2 and S3†) found in the literature into eqn (1),[8a,11] the equation can be derived to the following expression:

$$E_g^{CIGSSe}(x,y) = (0.98 + 0.167x^2 + 0.17y^2 + 0.023x^2y - 0.17xy^2 + 0.397xy + 0.31y + 0.523x)\ \text{eV} \quad (2)$$

This model could be used to determine the respective band gap energy for quinary CIGSSe at a given set of x and y. Fig. 4 shows a 3-D plot from the approximation model for the band-gap energy over the entire composition. The band gap values obtained from optical absorption edge, CV and the approximation model are listed in Table S4†. Both the values determined from optical band-gap edge and CV spectra match well with those obtained from the model.

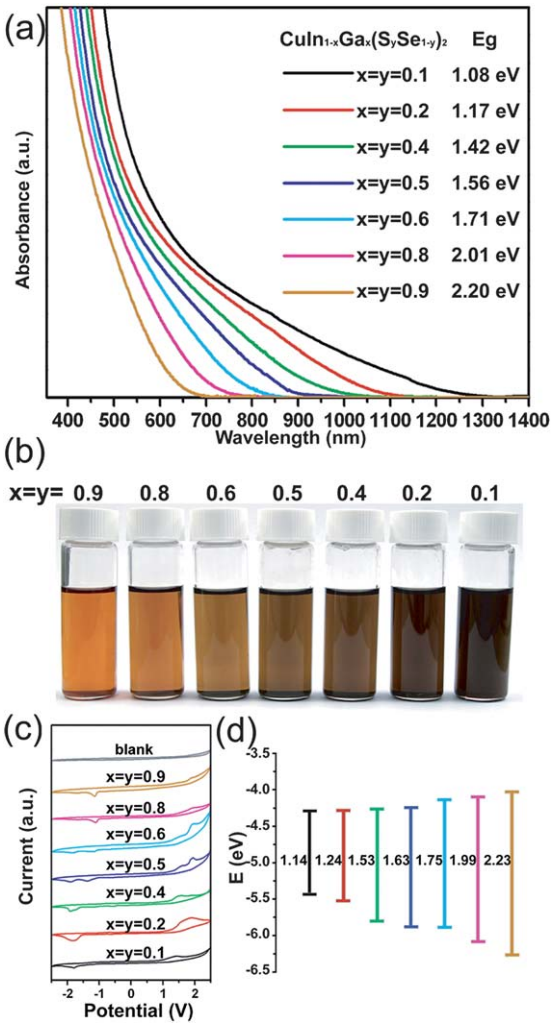

Fig. 3 (a) UV-visible-NIR absorption spectra and (b) photograph of $CuIn_{1-x}Ga_x(S_ySe_{1-y})_2$ nanocrystal solutions with varying In/Ga and S/Se ratios. (c) CV spectra and (d) determined energy levels of $CuIn_{1-x}Ga_x(S_ySe_{1-y})_2$ nanocrystals.

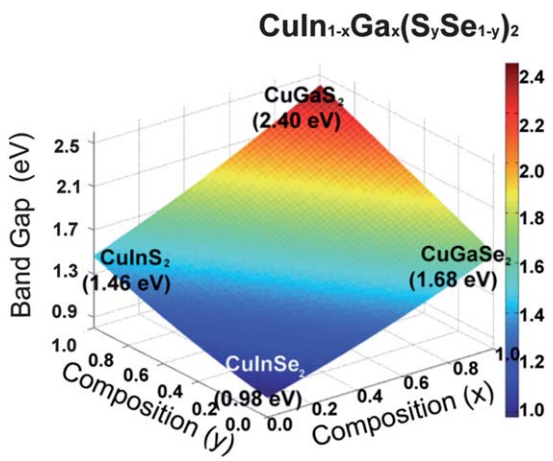

Fig. 4 Band gap energy diagram of the $CuIn_{1-x}Ga_x(S_ySe_{1-y})_2$ system in the range of $0 \leqq x \leqq 1$, and $0 \leqq y \leqq 1$ plotted based on eqn (2).

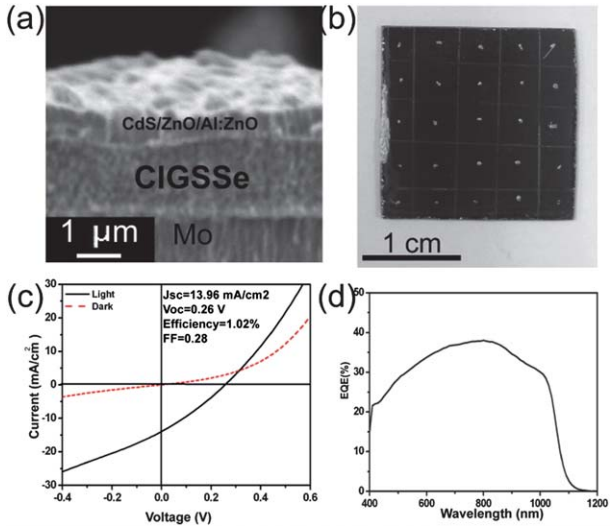

Fig. 5 (a) Cross-section image of a CIGSSe solar cell made by using CIGSSe nanocrystals as an absorber layer precursor. (b) Photograph of typical CIGSSe-based solar cell devices. (c) *J*–*V* characteristic and (d) EQE of a cell.

The obtained CIGSSe nanocrystals exhibit long-term dispersibility in organic solvents and are suitable for use in solution-processed thin film solar cells. We have incorporated inks based on the quinary nanocrystals into CIGSSe thin film solar cell fabrication. A p-type CIGSSe absorber layer was fabricated by spraying CIGSSe nanocrystals in toluene on a molybdenum-coated sodalime glass substrate followed by high-temperature annealing in a selenium atmosphere to sinter the nanocrystal film into larger grains. After the film was etched by KCN, the device was fabricated by sequential deposition of a CdS buffer layer, ZnO transparent layer, and top-electrode aluminium-doped ZnO (Al:ZnO) layer, forming a layered cell structure as shown in Fig. 5a. The devices had a cell efficiency of 1.02% with an active area of 0.15 cm^2 under AM 1.5 simulated sunlight. Device characteristics are as follows: V_{oc}: 0.26 V, J_{sc}: 13.96 mA cm^{-2}, and FF: 0.28. The low V_{oc} and J_{sc} obtained from the device indicates a more dominant recombination loss in the space charge region, probably due to film cracking and holes which cause electrons and holes to be trapped. External quantum efficiencies (EQE) of the cell in the complete wavelength range are shown in Fig. 5d, showing an efficient current spectral response at a wavelength in the infrared range. The special property of the cell is particularly pronounced for the wavelengths longer than 600 nm with the EQE as high as 38% at the wavelength 800 nm. The cell efficiency needs improvement, which is believed to be attainable by optimization of device fabrication processes.

The colloidal synthesis of quinary CIGSSe nanocrystals with entire composition tuning and band gap engineering in the range from 0.98 to 2.40 eV as well as their implementation into low-cost photovoltaic devices was achieved. CIGSSe nanocrystal inks represent a new type of absorber precursors for thin-film solar cell devices.

Acknowledgements

The authors acknowledge the financial support by the National Science Council of Taiwan (NSC 99-2221-E-007-096, NSC 100-3113-E-007-009-CC2, NSC 100-3113-E-007-008, NSC 100-2628-E-007-029-MY2), National Tsing Hua University (100N2060E1, 100N2041E1), the (Department of Industrial Technology) Ministry of Economic Affairs and Green Energy & Environment Research Laboratories, ITRI, Taiwan, and the HRTEM (JEOL JEM-2100F) assistance from Tamkang University College of Science.

Notes and references

1 (*a*) H. W. Hillhouse and M. C. Beard, *Curr. Opin. Colloid Interface Sci.*, 2009, **14**, 245–259; (*b*) Q. Guo, G. M. Ford, H. W. Hillhouse and R. Agrawal, *Nano Lett.*, 2009, **9**, 3060–3065; (*c*) Q. Guo, H. W. Hillhouse and R. Agrawal, *J. Am. Chem. Soc.*, 2009, **131**, 11672–11673; (*d*) A. Shiohara, S. Hanada, S. Prabakar, K. Fujioka, T. H. Lim, K. Yamamoto, P. T. Northcote and R. D. Tilley, *J. Am. Chem. Soc.*, 2010, **132**, 248–253; (*e*) J. Tang and E. H. Sargent, *Adv. Mater.*, 2011, **23**, 12–29; (*f*) Y. Xu, N. Al-Salim, C. W. Bumby and R. D. Tilley, *J. Am. Chem. Soc.*, 2009, **131**, 15990–15991; (*g*) M. J. Bierman and S. Jin, *Energy Environ. Sci.*, 2009, **2**, 1050–1059.

2 T. Todorov and D. B. Mitzi, *Eur. J. Inorg. Chem.*, 2010, **1**, 17–28.

3 (*a*) V. A. Akhavan, B. W. Goodfellow, M. G. Panthani, D. K. Reid, D. J. Hellebusch, T. Adachi and B. A. Korgel, *Energy Environ. Sci.*, 2010, **3**, 1600–1606; (*b*) B. D. Weil, S. T. Connor and Y. Cui, *J. Am. Chem. Soc.*, 2010, **132**, 6642–6643; (*c*) M. G. Panthani, V. Akhavan, B. Goodfellow, J. P. Schmidtke, L. Dunn, A. Dodabalapur, P. F. Barbara and B. A. Korgel, *J. Am. Chem. Soc.*, 2008, **130**, 16770–16777; (*d*) Q. Guo, S. J. Kim, M. Kar, W. N. Shafarman, R. W. Birkmire, E. A. Stach, R. Agrawal and H. W. Hillhouse, *Nano Lett.*, 2008, **8**, 2982–2987; (*e*) J. J. Choi, Y.-F. Lim, M. E. B. Santiago-Berrios, M. Oh, B.-R. Hyun, L. Sun, A. C. Bartnik, A. Goedhart, G. G. Malliaras, H. c. D. Abruña, F. W. Wise and T. Hanrath, *Nano Lett.*, 2009, **9**, 3749–3755.

4 (*a*) M. Yuan, D. B. Mitzi, O. Gunawan, A. J. Kellock, S. J. Chey and V. R. Deline, *Thin Solid Films*, 2010, **519**, 852–856; (*b*) V. Probst, W. Stetter, J. Palm, R. Toelle, S. Visbeck, H. Calwer, T. Niesen, H. Vogt, O. Hernandez, M. Wendl and F. H. Karg, *3rd World Conference on Photovoltaic Energy Conversion*, Osaka, 2003, vol. 1, p. 329.

5 Y. Chiba, S. Kijima, H. Sugimoto, Y. Kawaguchi, M. Nagahashi, T. Morimoto, T. Yagioka, T. Miyano, T. Aramoto, Y. Tanaka, H. Hakuma, S. Kuriyagawa and K. Kushiya, *Proceedings of the 35th IEEE Photovoltaic Specialists Conference*, New York, 2010, p. 164.

6 (*a*) J. J. Choi, W. N. Wenger, R. S. Hoffman, Y.-F. Lim, J. Luria, J. Jasieniak, J. A. Marohn and T. Hanrath, *Adv. Mater.*, 2011, **23**, 3144–3148; (*b*) Y. C. Lin, W. T. Yen, Y. L. Chen, L. Q. Wang and F. W. Jih, *Phys. B (Amsterdam, Neth.)*, 2011, **406**, 824–830; (*c*) S. P. Bremner, M. Y. Levy and C. B. Honsberg, *Progr. Photovolt.: Res. Appl.*, 2008, **16**, 225–233; (*d*) T. Ameri, G. Dennler, C. Lungenschmied and C. J. Brabec, *Energy Environ. Sci.*, 2009, **2**, 347–363.

7 (*a*) C. Eberspacher, C. Fredric, K. Pauls and J. Serra, *Thin Solid Films*, 2001, **387**, 18–22; (*b*) V. Alberts, J. Titus and R. W. Birkmire, *Thin Solid Films*, 2004, **451–452**, 207–211; (*c*) E. P. Zaretskaya, V. F. Gremenok, V. B. Zalesski, K. Bente, S. Schorr and S. Zukotynski, *Thin Solid Films*, 2007, **515**, 5848–5851.

8 (*a*) S.-H. Choi, E.-G. Kim and T. Hyeon, *J. Am. Chem. Soc.*, 2006, **128**, 2520–2521; (*b*) J. Tang, S. Hinds, S. O. Kelley and E. H. Sargent, *Chem. Mater.*, 2008, **20**, 6906–6910; (*c*) X. Wang, D. Pan, D. Weng, C.-Y. Low, L. Rice, J. Han and Y. Lu, *J. Phys. Chem. C*, 2010, **114**, 17293–17297; (*d*) M.-Y. Chiang, S.-H. Chang, C.-Y. Chen, F.-W. Yuan and H.-Y. Tuan, *J. Phys. Chem. C*, 2011, **115**, 1592–1599; (*e*) D. Pan, X. Wang, Z. H. Zhou, W. Chen, C. Xu and Y. Lu, *Chem. Mater.*, 2009, **21**, 2489–2493; (*f*) Y.-H. A. Wang, N. Bao, L. Shen, P. Padhan and A. Gupta, *J. Am. Chem. Soc.*, 2007, **129**, 12408–12409; (*g*) Y.-H. A. Wang, X. Zhang, N. Bao, B. Lin and A. Gupta, *J. Am. Chem. Soc.*, 2011, **133**, 11072–11075; (*h*) Y.-H. A. Wang, C. Pan, N. Bao and A. Gupta, *Solid State Sci.*, 2009, **11**, 1961–1964; (*i*) D. Pan, D. Weng, X. Wang, Q. Xiao, W. Chen, C. Xu, Z. Yang and Y. Lu, *Chem. Commun.*, 2009, 4221–4223.

9 (*a*) L. Vegard, *Z. Phys. A: Hadrons Nucl.*, 1921, **5**, 17–26; (*b*) G. H. Chapman, J. Shewchun, B. K. Garside, J. J. Loferski and R. Beaulieu, *Sol. Energy Mater.*, 1979, **1**, 451–469.

10 M. Bar, W. Bohne, J. Rohrich, E. Strub, S. Lindner, M. C. Lux-Steiner, C. H. Fischer, T. P. Niesen and F. Karg, *J. Appl. Phys.*, 2004, **96**, 3857–3860.

11 (*a*) S. H. Wei and A. Zunger, *J. Appl. Phys.*, 1995, **78**, 3846–3856; (*b*) *Handbook of Photovoltaic Science and Engineering*, ed. A. Luque and S. Hegedus, Wiley, 2003; (*c*) R. Noufi, R. Powell, C. Herrington and T. Coutts, *Sol. Cells*, 1986, **17**, 303–307.

